INDIAN JOURNAL OF SCIENCE AND TECHNOLOGY

RESEARCH ARTICLE

Magnesium-Doped Fluorophosphate Bioactive Glass For Bone Tissue Engineering: *In Vitro* and *In Vivo* Study

Jenifa Begam Rahumathullah[1], A S Priscilla[2], Pugalanthi Pandian Sankaralingam[3]*

1 Research Scholar, Department of Zoology & Research Centre, Lady Doak College, Madurai, Tamil Nadu, India
2 Assistant Professor, Department of Zoology & Research Centre, Lady Doak College, Madurai, Tamil Nadu, India
3 Managing Director, Bone Substitutes, 2/1088, Parijatham Street, Ezhil Nagar, Iyer Bangalow, Madurai, 625014, Tamil Nadu, India

OPEN ACCESS

Received: 28-07-2024
Accepted: 26-01-2025
Published: 14-03-2025

Citation: Rahumathullah JB, Priscilla AS, Sankaralingam PP (2025) Magnesium-Doped Fluorophosphate Bioactive Glass For Bone Tissue Engineering: *In Vitro* and *In Vivo* Study. Indian Journal of Science and Technology 18(9): 716-733. https://doi.org/10.17485/IJST/v18i9.2129

* **Corresponding author**.

pamc.mdu@gmail.com

Funding: M/S Pandian Advanced Medical Centre Private Limited, Madurai, India

Competing Interests: None

Published By Indian Society for Education and Environment (iSee)

ISSN
Print: 0974-6846
Electronic: 0974-5645

Abstract

Objectives: Owing to the ability of bioactive glasses to bond to the living bone, our study aims to take advantage of fluorophosphate glass systems over silicate-based systems in terms of controlled bioactivity and mechanical properties along with the utilization of therapeutic ions such as Mg^{2+}, and F^{-}. **Methods:** Melt-quenching method was used with varying mole concentrations of MgO. XPS, density by Archimedes principle, elastic moduli by ultrasonic, and thermal properties were characterized. *In vitro* bioactivity and release of osteo-stimulatory Mg^{2+} ions were assessed by SBF for 21 days followed by SEM-EDS, XRD, and FTIR. Biological evaluations included cell viability (MTT assay) using AGS, MG-63, and Human Endothelial Cell lines. Bone-forming capacity was assessed by ALP activity, and osteocalcin secretion in SaOS-2 and, MG-63. *In vivo* studies were conducted by using MgFP bioactive glass implant in rabbit femoral condyle and bone formation was analysed by SEM, EDS, and CLSM study. **Findings:** Optimal mechanical properties observed at 5 mol% MgO. *In vitro* investigation revealed compatibility with AGS, MG-63, and human endothelial cell lines. XRD analysis showed HAp formation at 31.92° designates successful conversion from amorphous to crystalline phase. The presence of ions such as Mg^{2+} and F^{-}, with a Ca/P ratio of 1.46 was confirmed by EDS analysis. MgFP5, with 5.0 mol% MgO, was chosen for *in vivo* evaluation to confirm the osteogenic capacity further. *In vivo* results showed a 67% bioconversion rate in the rabbits implanted with bioactive glass rod after 10 weeks of surgery, with no voids observed denoting resorption and new bone formation occurring at the same rate. **Novelty:** Our study indicates the benefits of cost-effective melt-derived Mg-doped fluorophosphate bioactive glass to treat critical load-bearing bone defects tested in rabbit models and addresses the limitations of conventional bioactive glass systems.

Keywords: Bone Graft Substitute; Hydroxyapatite Formation; Osteogenesis; Magnesium-Doped Fluorophosphate Bioactive Glass; In vitro and In vivo Bioactivity

1 Introduction

Probing efficient treatment methods for bone lesions due to accidental injuries, congenital abnormalities, and aging raises significantly worldwide. Existing usage of transplant procedures such as autograft, allograft, and xenograft were promising yet possessed several limitations in terms of donor availability, immune rejection, and the possibility of zoonotic infections. To overcome these hurdles, researchers developed synthetic biomaterials which have the advantage of optimization in the laboratory towards the clinical needs. The sources of synthetic biomaterials are unlimited, express high reproducibility, and have stable quality which reveals them as better alternatives than natural biomaterials. Initial synthetic biomaterials such as metals, ceramics, and polymers lacked the ability to support active tissue regeneration, limited in their ability to repair load-bearing bone defects, and led to complications such as immune rejection and stress shielding. Conventional silicate-based bioactive glasses have the disadvantage of slower dissolution rate, less stable pH control, reduced flexibility in mechanical properties, risk of excessive bone formation, and less susceptible to modification[(1)]. Phosphate-based bioactive glasses considered as third-generation biomaterials provided the advantage of tailoring the composition to meet specific structural needs over silicate-based glass systems. The physical, chemical, and biological properties of the phosphate-based glasses could be altered by varying the ratios of elements such as calcium, sodium, and phosphorus to gain a closer resemblance to the complexity of natural tissues. Among the available methods for the preparation of bioactive glasses, previous studies reported the sol-gel method which involves multiple, time-consuming steps, exhibits reduced reproducibility and scalability, and is often more expensive due to processing requirements. Employing melt-quenching method was reported to result in high homogeneity and purity of the bioactive glasses due to processing at high temperatures, better control over porosity and density, superior mechanical properties, suitable for large-scale production with high reproducibility, and less expensive[(2)].

Recent advancements have probed the incorporation of therapeutic ions such as fluoride and magnesium into phosphate-based bioactive glasses which maximize medical efficiency. Fluorides are known to stimulate osteoblast cells at moderate concentrations (25–500 μg mL^{-1}), but higher concentrations (<500 μg mL^{-1}) may suppress osteoblastic activity[(3)]. Magnesium (Mg) is an alkaline earth metal that is present intracellular in the human body with a total content of about 24 g (1 mole) per 70 kg predominantly located in the bones and soft tissues. Mg has the ability to reduce fracture risk in osteoporosis treatments, increase bone density, and engage in bone repair as it inhibits osteoclast activity and increases osteoblast activity. Mg^{2+} ions are present by 1.11 weight % in dentin and 0.47 weight % in bones and play essential roles in the human body as they take part in biological and biochemical processes and maintain the cytoskeletal integrity through proteins and nucleic acid synthesis, active calcium transport, phagocytosis, bone tissue development, and remodelling. Mg acts as a cofactor for enzymes such as matrix metalloproteinases (MMP) and vascular endothelial growth factor (VEGF) which promotes blood vessel formation and increases the production of nitric oxide (NO), a vasodilator that also initiates the Notch Signalling Pathway associated with angiogenesis[(4)]. Furthermore, MgO can modify the physical, mechanical, and thermal properties of phosphate-based glass systems.

Existing studies are limited to the *in vivo* interactions, particularly in rabbit models which also failed to address the long-term evaluations of melt-derived Mg-doped

phosphate-based bioactive glass implants. Our present study aims to correct the gap between expensive processing methods and less efficient glass systems, by utilizing an efficient and cost-effective melt-derived method for the preparation of Mg-doped fluorophosphate bioactive glass. It exploits the advantage of phosphate-based system over a previously reported silicate-based glass system. The lack of targeted treatment options leads to prolonged healing time and incomplete recovery[5]. In order to provide innovative targeted treatment options, this study aims at the development of melt-derived Mg-doped fluorophosphate bioactive glass that was implanted in rabbits to manage and address critical bone defects, particularly in load-bearing applications.

2 Methodology

2.1 Formulation and preparation of bioactive glass composition

The $45P_2O_5$-29CaO-2.5CaF_2-22.5-XNa_2O-MgO bioactive glasses at various mole concentrations were prepared by melting the homogeneous mixture of phosphate, calcium, sodium, fluoride, and the metal oxide salt (MgO) followed by sudden quenching of the melt. The required inorganic chemicals, listed in Table 1, were obtained from Sigma-Aldrich, India. The sample code (MgFP1, MgFP2, MgFP3, MgFP4, and MgFP5) and the compounds for preparing the bioactive glasses were precisely weighed as shown in Table 1. Magnesium was taken in the form of its oxide (MgO) at 1 mol % to 5 mol %. The ratio of Ca:P was kept as constant. CaF_2 was kept at a constant of 5% mole of fluorine which has been proved to be the ideal concentration for fluorine. MgO was added at the sacrifice of Na_2O so that the bioactive elements remained unchanged. In a ball mill, the mixture was ground well and then preheated (100-120°C) in an aluminium crucible for 1 hr. The materials were preheated and cooled to 37°C before being subjected to further grinding in a ball mill, resulting in the formation of a homogenous compound. The mixture was taken in a platinum crucible (10% rhodium doped) and melted at a temperature ranging from 1050 °C to 1400 °C for 1 h in an electric furnace. The temperature in the furnace was kept constant throughout the process. The melt was poured into a preheated graphite/ steel mould and cooled to room temperature. The prepared glasses were made into cylindrical rods (2 mm diameter) for *in vivo* studies and sliced using a diamond saw for *in vitro* characterization.

Table 1. Chemicals and their mole percentage of magnesium-doped fluorophosphate bioactive glasses

	Concentration (mol %)				
Sample Code	**P_2O_5**	**CaO**	**MgO**	**Na_2O**	**CaF_2**
MgFP1	45.00	29.00	1	22.50	2.50
MgFP2	45.00	29.00	2	21.50	2.50
MgFP3	45.00	29.00	3	20.50	2.50
MgFP4	45.00	29.00	4	19.50	2.50
MgFP5	45.00	29.00	5	18.50	2.50

2.2 Characterization of magnesium fluorophosphate bioactive glasses

2.2.1 Surface characterization

The elemental composition of the prepared bioactive glass was analyzed using X-ray photoelectron spectroscopy (XPS) (model: AXIS Ultra DLD; Kratos, Kyoto, Japan), employing Al Kα as the excitation source and operating at a power of 210 W. A survey spectrum was recorded across the energy range of 0-1200 eV, and high-resolution spectra were obtained for the C1s and N1s peaks. The XPS measurements were conducted in a fixed retarding ratio mode with a bandpass energy of approximately 10 eV using X-ray as an excitation radiation.

2.2.2 Mechanical and thermal characterization

The density, mechanical, and thermal properties of the bioactive glasses were further analysed. The density of the magnesium-doped bioactive glass pellets was determined through the conventional Archimedes' principle, with a precision of ± 0.5 kg/m^3. The Young's, longitudinal, shear, and bulk moduli of the prepared bioactive glass pellets were assessed by measuring the ultrasonic velocities using an ultrasonic process control system (Model FUII050; Fallon Ultrasonics Inc., Ltd., Ontario, Canada) and a 100-MHz digital storage oscilloscope (Model 54600B; Hewlett Packard, Palo Alto, California, USA), utilizing the pulse-echo method and cross-correlation technique. The thermal stability of the bioactive glasses was investigated using Simultaneous Thermal Analysis (STA 449 F3Nevio). Around 3.5 mg of the sample was heated to 1000°C at a rate of 10°C min^{-1} under nitrogen atmosphere.

2.3 Assessment of Bioactivity

The analysis of the bioactive nature of the prepared samples was carried out through immersion in simulated body fluid (SBF). The SBF solution was formulated using the method developed by Kokubo *et al.*,[6] which assures that the inorganic ion concentrations closely matched those found in human body fluids. The SBF solution was prepared through the dissolution of high-purity analytical grade salts, such as NaCl, KCl, $NaHCO_3$, $MgCl_2 \cdot 6H_2O$, $CaCl_2$, and KH_2PO_4, in double distilled water at a temperature of 37°C. Following this, the pH of the solution was buffered to 7.4 using TRIS [tris(hydroxymethyl) aminomethane] and 1N HCl. Subsequently, the MgFP samples were immersed in the SBF solution and incubated at 37°C in a 5% CO_2 incubator for 21 days. Throughout the incubation period, the pH of the SBF solution was recorded daily using a pH meter (Thermo Scientific™ Orion™ 3-Star Benchtop). After the 21-days incubation, the samples were retrieved for further analysis. Fourier transform infrared (FTIR) spectroscopy (model: 8700; Shimadzu, Tokyo, Japan) was employed to obtain the absorption spectra of the prepared specimen after the *in vitro* studies, using the potassium bromide (KBr) pellet technique within the wavenumber range of 4000–400 cm^{-1}. This analysis assisted in understanding the functional groups present in the samples. X-ray diffraction (XRD) analysis (PW 1700; Philips, Eindhoven, The Netherlands) was carried out to confirm the crystalline nature of the samples and to detect the formation of a hydroxyapatite (HAp) layer on the surface after the *in vitro* incubation. Furthermore, MgFP5 bioactive glass with superior bioactivity (based on FTIR and XRD) was analysed for the surface morphology and elemental composition, both before and after immersion in SBF, using scanning electron microscopy (SEM) (model: 514A; Zeiss, Oberkochen, Germany) and energy dispersive X-ray spectroscopy (EDAX) (model: Oxford Xmax50 EDS, Oxford Instrument, England).

2.4 Biological evaluation

2.4.1 Cell culture maintenance

The MG-63 (human osteoblast-like) cell line was procured from ATCC (American Type Culture Collection). The cell line was cultured in Minimum Essential Media (MEM) supplemented with 10% Foetal Bovine Serum (FBS), 50 U/ml penicillin, 50mg/mLstreptomycin, and 1% L-glutamine (Gibco). Cells were cultured in T25 flasks (Nunc, USA) in a humidified CO_2 incubator (Heraeus, Germany) with 5% CO_2 at 37°C. Accutase (Gibco) was used to trypsinize the cells and cultured them subsequently.

2.4.2 Cell viability assay

The MG-63 cells at the concentration of 1×10^4 were pre-seeded in a 96-well plate. The MgFP glasses were dissolved in deionized water and the ionic dissolution products of MgFP bioactive glass samples with various concentrations were added to the wells in triplicates using phenol red-free, serum-free, antibiotic-free media. The wells without the addition of samples were maintained as controls. The plates were incubated in a CO_2 incubator with 5% CO_2 at 37°C for 24 and 48 h. Four hours before the assessment, 3-[4,5- dimethylthiazol-2-yl]-2,5-diphenyl tetrazolium bromide (MTT) (Himedia, India) dye which had been prepared in phosphate-buffered saline (PBS) at the concentration of 5mg/mL was added to the wells. Dimethyl sulfoxide (DMSO) 200 μL was added to the wells at the end of 4 h to dissolve the crystal formation. The purple-coloured formazan was observed and read at 570 nm in an ELISA reader (Robonik, India). Cell viability percentage was calculated by the optical density (OD) value in sample wells (cells with ionic dissolution products of fluorophosphate bioactive glasses) divided by the OD value in control wells (only cells without treatment of the samples), multiplied by 100.

$$Cell\ viability\ \% = \frac{Mean\ OD\ value\ of\ samples - OD\ of\ blank}{Mean\ OD\ value\ of\ \text{control} - OD\ of\ blank}\ X\ 100$$

2.4.3 Alkaline phosphatase assay

The ALP activity was assessed by p-nitrophenyl phosphate (pNPP) method by using a commercial kit (SensoLyte® pNPP Alkaline Phosphatase Assay Kit Colorimetric, USA). MG-63 cells were pre-seeded at the concentration of 1 X 10^6 in 24 well culture plates and incubated for 48 hours at 37°C in a 5% CO_2 incubator. After reaching confluence, the MG-63 osteoblast cells were treated with varying concentrations of MgFP (0.1 to 100 μg/mL) and incubated for 48 hours. After the incubation period, the cells were washed twice with ice-cold PBS and homogenized in 50 μL of assay buffer. Following this step, the insoluble components were removed by centrifugation at 177 g-force for 3 minutes. The ionic dissolution products of the experimental samples with different MgFP concentrations (0.1, 1, 10, and 100 μg/mL) were then added to a 96-well plate, followed by the addition of 10 μL of ALP enzyme. Each well was added with 50 μL of 5 mM p-nitrophenyl phosphate (pNPP) solution. The reaction mixture was incubated for 60 minutes at 25°C in the dark. The reaction mixture was left to incubate in the dark for 60

minutes at 25°C. The reaction was stopped by adding 20 μL of stop solution, and the optical density (OD) values were recorded at 405 nm by using a microplate reader.

2.4.4 Osteocalcin secretion

MG-63 osteoblast cells were cultured and seeded on a 24-well plate at a density of 2×10^5 cells per well. After allowing the cells to attach to the plate (approximately 18 to 24 hours), the spent media was removed, and the cells were washed with Dulbecco's phosphate-buffered saline (DPBS). To synchronize the cells, serum starvation was performed for approximately 18 to 24 hours in order to synchronize the cells by adding serum-free, antibiotic-free, and phenol-red-free medium. MgFP stock solution was homogenized prior to the preparation of the experimental concentrations (1, 10, and 100 μg/mL) in the cell culture media. The solutions with the prepared concentrations were added in duplicate to the corresponding wells and incubated for 48 hours. The extracellular media from all samples with varying MgFP concentrations was collected in microcentrifuge tubes in triplicates and immediately chilled to prevent the degradation of osteocalcin by proteases. The cells were then washed with DPBS and treated with 500 μL of cell lysis solution (specific volume for 10^6-10^7 cells). The plate was gently agitated for 15 minutes and observed under the microscope to ensure complete cell lysis. The lysed components were also collected and placed in a cold environment to protect osteocalcin from degradation. Both the extracellular media and cell lysate samples were centrifuged at 177 g-force for 20 minutes at 4°C. The supernatants were then used for the osteocalcin quantification assay. The 25 μL aliquot of the calibrator, control, and test samples was added to the appropriate wells of an ELISA plate, followed by the addition of 100 μL of the working anti-OST-HRP conjugate. The plate was left to incubate at 37°C for 2 hours. The liquid was then aspirated, and the plate was washed thrice with the working wash solution of 400 μL each time and aspirated from each well. Subsequently, 100 μL of the chromogenic solution was added to each well, and the plate was incubated for 30 minutes at 37°C in the dark. The reaction was stopped by adding 100 μL of the stop solution, and the absorbance was measured at 450 nm (with a reference filter at 630 nm or 650 nm) within 1 hour using a microplate reader (Readwell Touch Robonik ELISA Plate Reader, India).

2.4.5 Statistical analysis

The data are expressed as the mean $\pm$ standard deviation. Statistical analysis was carried out using GraphPad Prism software. Independent t-tests, one-way ANOVA, or two-way ANOVA were applied for multiple comparisons between groups followed by Tukey's Honest Significant Difference test (post-hoc test) as appropriate. Statistical significance was defined as a P-value of 0.05 or less ($p < 0.05$). All experiments and assays were conducted in three technical replicates.

2.5 In vivo studies

The experiments were conducted at a designated animal facility (Animal House Facility, Lady Doak College, Madurai) with ethical approval (Approval number IAEC-LDC/8/14/1). Young male rabbits of similar weight and age (New Zealand White strain, *Oryctolagus cuniculus*, approximately 1.6 kg) were obtained from an authorised supplier (King Institute, Chennai). Their care was adhered to established guidelines (CPCSEA guidelines). Anaesthesia (ketamine and sevoflurane) was administered before making a small incision (1 cm) over the femur's medial epicondyle (guided by imaging). The surgical site was magnified, and a narrow-angled drill (2 mm) was used to create a hole while continuously irrigating the area with saline solution. A specific bioactive glass material (MgFP5 bioactive glass, 2 mm diameter) with superior bioactivity (based on *in vitro* tests) was pegged into the hole. After rinsing with saline, the wound was sutured with single-layer sutures (3–0 Ethilon sutures, Johnson & Johnson, England). A single dose of antibiotic (ceftriaxone, 250mg) was administered intramuscularly. Following anaesthesia recovery, the rabbit was allowed free movement. To label newly formed bone, a fluorescent marker (calcein, Sigma Aldrich, Japan) was injected intramuscularly on the surgery day and then weekly until two days before euthanasia (10 mg/kg dose). After ten weeks, the rabbits were euthanized using lethal dose of ketamine. The lower end of femur was harvested and preserved in formalin (10% solution). The specimen was subsequently dried and embedded in a resin (methyl methacrylate, MMA). Using a specialized microtome (Model SP1600, Leica, Germany), undecalcified sections with a thickness of 100 μm were obtained perpendicular to the implanted rod. These sections were examined by using various techniques (EDS, SEM, CLSM). The undecalcified specimen was dried at 37°C and coated with a thin gold film using a sputtering technique. Measurements of the glass and interface size were taken at various magnifications (100X and 200X). The dried specimen was analysed using a scanning electron microscope (SEM, Model Ultra 55; Zeiss, Oberkochen, Germany) coupled with an energy dispersive spectroscopy (EDS, Model Oxford Xmax50 EDS; Oxford Instruments, England) to assess the formation of HAp at the bioceramic-bone interface. To obtain semi-quantitative information about the elements present at the newly formed bone-glass interface, an energy dispersive spectrometer (EDS Model X-mas 50mm^2, Oxford Abingdon, England) was employed. The CLSM (Model: Fluoview-1x70, Olympus, Japan) was used to assess cellular infiltration and tissue patterns within the implanted glass. Excitation with an argon (Ar) laser at 488 nm allowed for the detection of metabolically active cellular infiltration through

a specific filter (515–565 nm bandpass filter), appearing as bright green fluorescence.

3 Results

3.1 Surface, mechanical and thermal characterization

Table 1 unveils the elemental composition of the prepared material. The Ca/P ratio was maintained at a constant 1:3 ratio. Calcium fluoride (CaF_2) was added to achieve a fluoride concentration of 5%, which is based on our previous work[7]. Furthermore, sodium oxide (Na_2O) acts as a network modifier and that was modified by replacing it with magnesium oxide (MgO) in varying amounts ranging from 1 to 5 mol%. In XPS evaluation (A), peaks at 28 eV and 523 eV suggest Calcium Fluoride (CaF_2) in the glass matrix, which contributed to the bioactivity and structural integrity of the glass. The presence of fluoride in the form of CaF_2 is advantageous which promotes the bone-forming capability of the bioactive glass. Peaks at 89.2 eV and 349.8 eV indicate Phosphorus (P), and the presence of phosphorus pentoxide (P_2O_5) at 187.7 eV, indicates its critical role that forms the phosphate network necessary for the bioactivity of the glass. Magnesium (Mg) confirmed its presence in the MgFP bioactive glass which has a characteristic peak of around 118.2 eV binding energy that denotes improved mechanical properties and enhanced bioactivity. Calcium Oxide (CaO) identified at 151.3 eV, affects the dissolution rate of the glass and aids in the formation of a hydroxyapatite (HAp) layer. Sodium Metaphosphate ($NaPO_3$) and Sodium Oxide (Na_2O) were detected at 533.5 eV and 1072.5 eV, respectively, and these compounds modify the glass structure and enhance its solubility, which is suggestive of the bioactivity and gradual dissolution of the glass in biological environments[8].

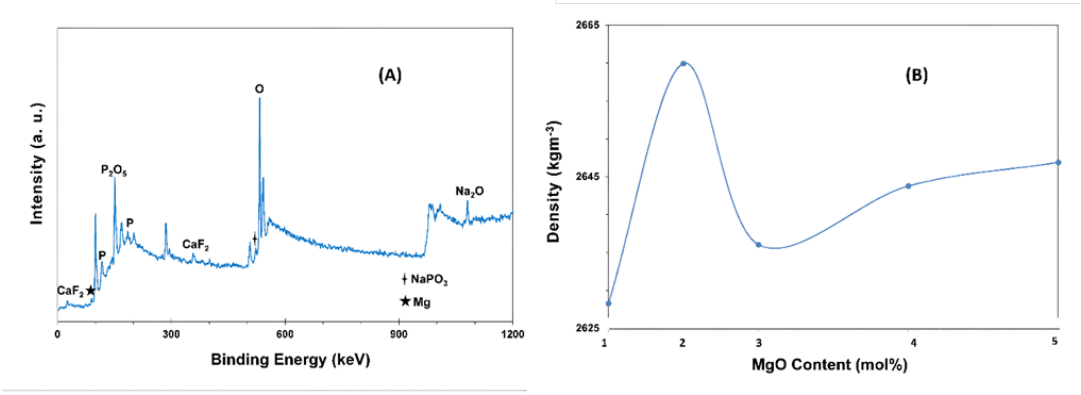

Fig 1. (A) XPS spectrum of the magnesium-doped fluorophosphate bioactive glass (MgFP5). (B) Density variation of Mg-doped bioactive glasses having different mol % of MgO

Table 2. XPS transmittance energy for the MgFP5 fluorophosphate bioactive glass sample

S.No	Binding Energy (eV)	Spectral Line	Compound
1	28	Ca 2p	CaF_2
2	89.2	P 2p	Phosphorus (P)
3	118.2	Mg 1s	Magnesium (Mg)
4	151.3	Ca 2p	Calcium Oxide (CaO)
5	187.7	P 2p	P_2O_5
6	349.8	P 2p	Phosphorus (P)
7	523	Ca 2p	CaF_2
8	533.5	Na 1s	Sodium Metaphosphate ($NaPO_3$)
9	1072.5	Na 1s	Sodium Oxide (Na_2O)

The density graph depicts the relationship between the density of bioactive glass and the mol% concentration of MgO (Figure 1**(B)**). Initially, the density sharply increases up to around 2 mol% MgO where the density peaks around 2659 kg/m^3. Subsequently, beyond 2 mol%, there is a decline in density, hitting a minimum of around 4 mol% with a peak density of 2643 kg/m^3, followed by a slight increase at 5 mol% to 2645 kg/m^3.

Following the density study, the pulse-echo method was employed to measure the elastic moduli (Longitudinal, Bulk, Young's, and Shear) (Figure 2 and Table 3), and that provides insights into the biomaterial's strength and interatomic potential. Young's Modulus shows a peak around 49.6 GPa for 2 mol% MgO, which aligns with the density peak suggesting that the material is stiffer due to more effective atomic packing. Bulk Modulus also peaks around 45.1 GPa in 2 mol% and declines and reaches to the minimum near 4 mol% at 38.4 GPa, then increases again to 47 GPa. This suggested the material is more resistant to compression at lower MgO contents. Longitudinal Modulus shows a trend that resembles the Young's Modulus, peaking around 47.9 GPa in 1 mol% which indicates maximum rigidity at this composition. Shear Modulus (G) exhibits less variation but shows an overall decrease, with a small peak around 18.87 GPa for 5 mol%.

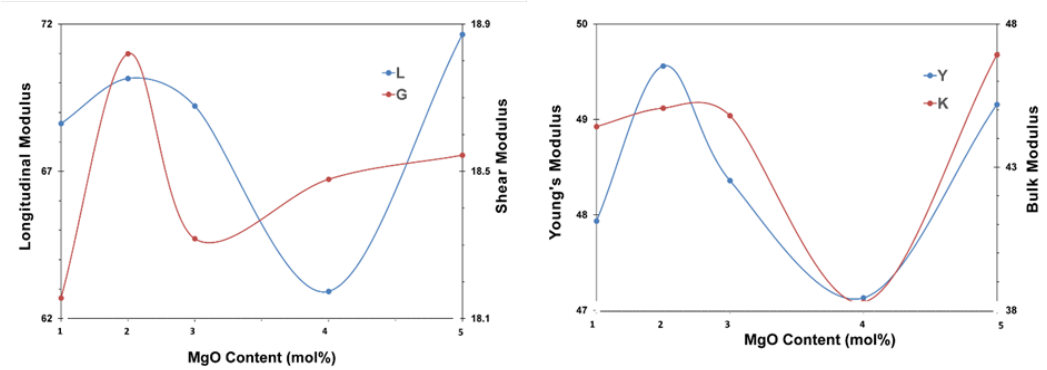

Fig 2. Longitudinal, Bulk, Young's, and Shear moduli variation in Mg-doped fluorophosphate bioactive glasses having different mol % of MgO

Table 3. Density (ρ), longitudinal modulus (L), bulk modulus (K), Young's modulus (Y), shear modulus (G), and Poisson's ratio (σ) for Mg-doped bioactive glasses having different amounts of MgO

MgO Content (mol%)	Density (kg/m^3)	Longitudinal Modulus (L-GPa)	Bulk Modulus (K-GPa)	Young's Modulus (Y-GPa)	Shear Modulus (G-GPa)	Poisson's Ratio (σ)
1	2627	62.7	43.6	47.9	18.64	0.285
2	2659	70.9	45.1	49.6	18.75	0.323
3	2637	64.5	45	48.3	18.7	0.292
4	2643	66.5	38.4	47.1	18.18	0.295
5	2645	67.2	47	49.1	18.87	0.301

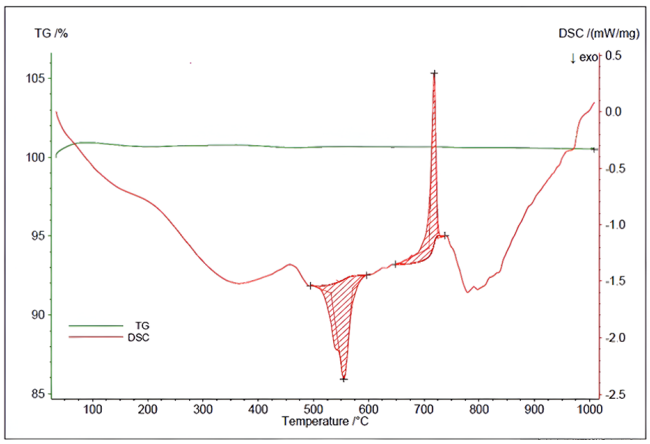

Fig 3. DSC and TG curves for the Mg-doped fluorophosphate bioactive glass (MgFP5)

Thermal transitions such as crystallization and melting (Figure 3) were analysed by differential scanning calorimetry (DSC) curve. The exothermic peak corresponds to the crystallization process (Tc), while the endothermic peak indicates the melting point (Tm) of the glass matrix. A sharp exothermic peak around 555°C, indicating the crystallization temperature. The area under the crystallization peak is -171.1 J/g, represents the associated enthalpy of crystallization (ΔHc) which indicates the energy released during crystallization. The endothermic peaks at 713.4°C and 837.2°C, correspond to melting transition and the enthalpy of fusion (ΔH_f) represents the areas of the endothermic peaks at 72.7 J/g and 104.6 J/g respectively, which indicates the energy absorbed during melting[8].

3.2 Assessment of bioactivity in SBF

3.2.1 pH variations in SBF

Figure 4 represents the change in pH of SBF after immersion of the samples for different periods (continuously from day 1 to 21). The pH behaviour of SBF can assess the mechanism of HAp formation after immersion of the samples. All MgFP sample compositions presented an abrupt decrease in the pH of the simulated body fluid (SBF) during the initial period. This rapid drop in pH is likely caused by the formation of phosphoric acid due to the dissolution of the glass samples. By the fifth day of immersion, the release of alkaline earth metal ions, such as sodium (Na^+) and/or calcium (Ca^{2+}), from the glass structure increased the pH of the SBF. This increase in pH can be due to the replacement of H^+ ions by the cations which resulted in a higher concentration of hydroxyl (OH^-) ions. The phosphate network (P_2O_5) is the primary network of the glass that is attacked and broken down through hydrolysis, which is facilitated by the higher pH of the SBF, leading to the cleavage of P-O-P bonds, releasing phosphate ions (PO_4). The decrease in pH observed was a result of calcium (Ca^{2+}) and phosphate (PO_4^{3-}) ions absorption from the SBF which facilitated the HAp layer formation on the surface of the MgFP bioactive glasses. This reduction in pH reveals the consumption of hydroxide (OH^-) ions during the HAp precipitation process. The released phosphate and calcium ions react with the ions in the SBF (which mimics the ionic concentration of human blood plasma) to form a HAp layer on the glass surface[9]. On the fifth day, the MgFP5 sample had the highest pH compared to all the other compositions and the MgFP1 sample showed the lowest pH value at day 21.

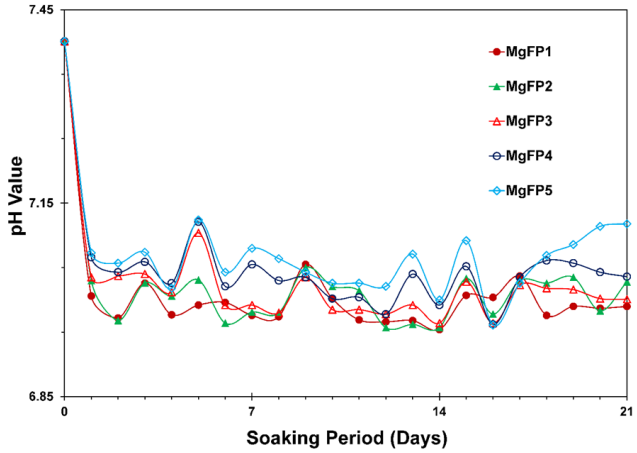

Fig 4. pH variations of Mg-doped fluorophosphate bioactive glasses (MgFP1, MgFP2, MgFP3, MgFP4, and MgFP5) in SBF solution during *in vitro* studies for 21 days soaking period

3.2.2 XRD pattern

Figure 5(**A**) represents the XRD patterns of prepared bioactive glass samples (MgFP1, MgFP2, MgFP3, MgFP4, and MgFP5). Each MgFP samples show distinct peaks at 2θ values which indicates the presence of crystalline phases. The characteristic peaks for MgFP bioactive glasses are found in the range of 20° to 80° 2θ. Peaks around 26° and 32° at 2θ values are characteristic of HAp which denotes that the bioactive glasses have successfully facilitated the formation of this phase, which is essential for bone regeneration[10]. Successful HAp formation is inferred because of the well-defined peak around 26°2θ which indicates the presence of a crystalline phase in MgFP1 that corresponds to HAp. A high degree of crystallinity in MgFP1 is expressed by the overall pattern. The XRD pattern in MgFP2 shows multiple sharp peaks, with prominent peaks around 26° and 32° 2θ which

suggests more than one crystalline phase formation. The 26° and 32° 2θ peaks in MgFP2 designate HAp formation. MgFP3 shows fewer and less intense peaks around 26°2θ compared to MgFP1 and MgFP2 indicates a lower degree of crystallinity and a more amorphous structure with some crystalline regions. MgFP4 exhibits well-defined peaks similar to MgFP2, characterized by distinct peaks around 26° and 32° 2θ which represents a significant crystalline content that confirms the presence of HAp formation. MgFP5 shows a distinct peak around 26° 2θ accompanied by additional peaks of lower intensity. The peaks are broader than MgFP1 and MgFP2, which denotes a mix of crystalline and amorphous phases. The broad peaks of MgFP5 indicate higher crystallinity but there is still a notable presence of HAp formation as indicated by the peak at 26° 2θ. MgFP5 has a mix of crystalline and amorphous phases, which can be because of the gradual release of ions and sustained bioactivity. Mg^{2+} acts as a network modifier, disrupting the glass structure and facilitating the nucleation and growth of HAp crystals as supported by the results of pH variations of the present study. This enhancement is remarkable compared to fluorophosphate bioactive glasses without magnesium doping, as it results in faster and more efficient HAp formation [9].

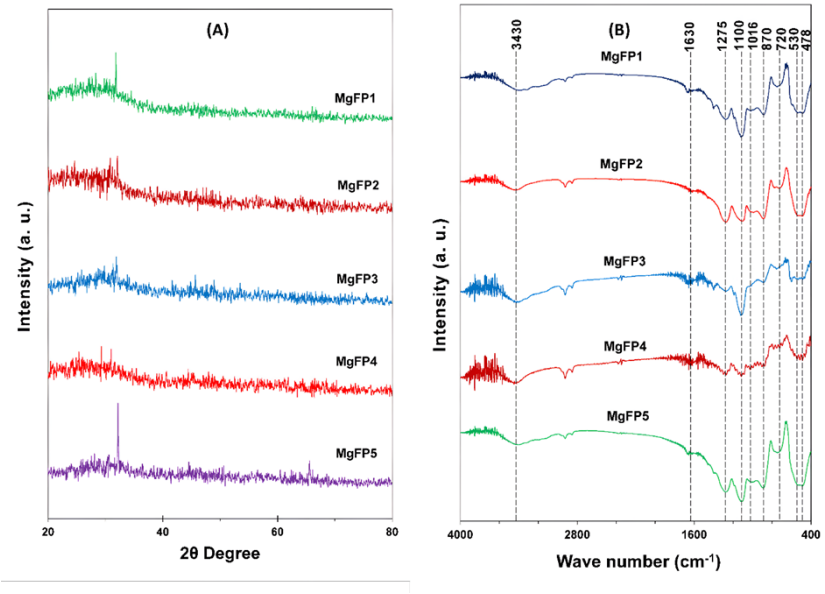

Fig 5. (A).XRD patterns of Mg-doped fluorophosphate bioactive glasses (MgFP1 – MgFP5) after bioactivity test. (B).FTIR peaks of the Mg-doped fluorophosphate bioactive glasses after 21 days *in vitro* test in SBF

3.2.3 FTIR analysis

The FTIR analysis of the MgFP1 to MgFP5 samples after in vitro studies is shown in Figure 5(**B**). The functional groups that are essential for bone-bonding ability are highlighted by the wavenumbers and their corresponding assignments which are associated with HAp and related phosphate compounds. The O-H stretching vibrations from water molecules linked to HAp are indicated by the broad peak at 3430 cm^{-1} which is present in all samples and confirms the consistent presence of water, which is important for the bioactivity of the glass samples. The H-O-H bending peak at 1630 cm^{-1} provides additional evidence that adsorbed water is present in all samples. The phosphate groups (PO_4^{3-}) in HAp are characterized by P-O bending vibrations, which are designated by the absorption band at 478 cm^{-1} and 530 cm^{-1}. The peaks at 1275 cm^{-1} and 1100 cm^{-1} correspond to asymmetric stretches of PO_2 and P-O-P, respectively. This band indicates the presence of calcium pyrophosphate (Ca_2P_2O) groups within the material. These vibrations are critical indicators of the phosphate framework essential for the bone-forming ability. The presence of phosphate groups in the samples is further confirmed by the 1016 cm^{-1} peak, which corresponds to P-O stretching vibrations [11].

Table 4. FTIR interpretation of Mg-doped bioactive glasses after 21 days *in vitro* test in SBF

Wavenumber (cm^{-1})	Assignment
3430	O-H stretch (water in HAp)
1630	H-O-H bend (absorbed water)
1275	P=O asymmetric stretch

Continued on next page

Table 4 continued

1100	P-O-P asymmetric stretch (calcium pyrophosphate - Ca_2P_2O)
1016	P-O stretch (HAp and FAp)
870	C-O stretch
720	P-O-P symmetric stretch
530	P-O bend (HAp)
478	P-O bend (phosphate ion - PO_4^{3-})

3.2.4 SEM-EDS analysis

Figure 6 represents the SEM image of the MgFP5 sample, which denotes the glassy nature before immersion in SBF. The SEM micrograph of the prepared material appears smooth on the surface and featureless which indicates a homogenous material with no significant surface irregularities or deposits and exhibited an amorphous nature before immersion in SBF. The EDS spectra of MgFP5 which denotes the elements P, Ca, Na, F, O, and Mg are present on the sample surface and their atomic and weight percentages have been presented in Figure 6 (**A1 & B1**) before and after immersion. Before and after immersion (in SBF for 21 days) SEM micrographs of the MgFP5 bioactive glass show the presence of crystalline deposits which denotes a significant change in surface morphology due to immersion in SBF. The formation of these crystalline structures suggests the precipitation of new phases on the bioactive glass surface. The EDS analysis performed on the surface of MgFP5 after immersion in SBF for 21 days (Figure 6 B1) shows that the surface contained Ca, and P having low-intensity peaks attributed to the absorption of Ca^{2+} and PO_4^{3-} to the formation HAp precipitation which was supported by the results of pH variation in the present study. The released phosphate and calcium ions reacted with the ions in the SBF to form HAp layer on the glass surface. The EDS spectra further confirmed the growth of HAp crystals on the surface of the samples after immersing in SBF [12]. The detection of fluoride molecules in the surface precipitate confirms the presence of fluorapatite (FAp). Hence, the EDS spectrograph reveals both HAp and FAp on the MgFP5 glass sample surface.

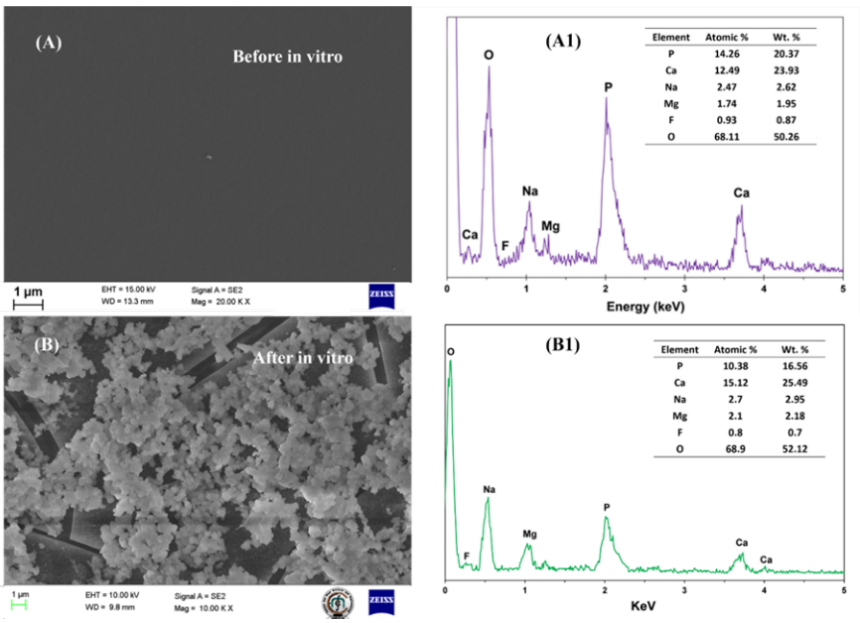

Fig 6. SEM_EDS spectra for the Pre-immersed (A & A1) and Post-immersed (B & B1) sample – MgFP5

3.3 Biological evaluation

3.3.1 MTT assay

Based on the *in vitro* evaluation in simulated body fluid (SBF) and the assessment of mechanical properties, the MgFP5 bioactive glass which demonstrated improved bioactivity and better mechanical strength was selected for further biological investigation. The *in vitro* cytotoxicity was performed using human gastric carcinoma (AGS) cell line (ATCC-1739), osteoblast-like cell line MG-63 (ATCC-1427), and Human Endothelial cells (ATCC-PCS-100-010) to assess cell viability by MTT assay. Human gastric

adenocarcinoma (AGS) cell line was obtained from the National Centre for Cell Science in Pune, India. The confluent cells were seeded at a density of 10^3 cells per mL. The cells were exposed to increasing concentrations of MgFP up to 100 μg/ mL. The percentage of viability was calculated based on the optical density (OD) at 590 nm by analysing the MgFP-treated cells to untreated controls. The cell viability percentage was determined after incubating the cells with different sample concentrations for 48 hours at 37°C in a 5% CO_2 environment. The cell viability was calculated by considering the viability of all 3 cell lines cultured in cell culture medium without antibiotic and serum as 100%. The results recommended that the highest cell viability after 48 hours of exposure to the samples at a concentration of 0.1 μg/mL was (86.35 $\pm$ 0.59) %, (76.49 $\pm$ 0.68) %, and (80.23 $\pm$ 0.92) % for AGS, MG-63, and Human Endothelial cell line respectively as shown in Figure 7.

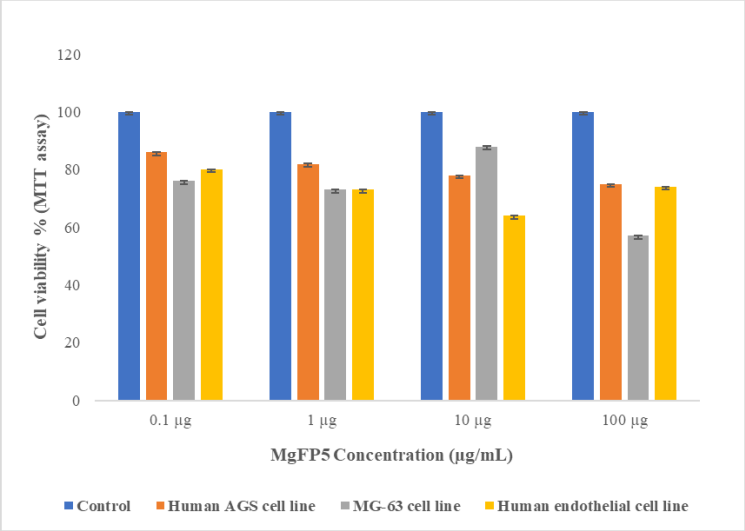

Fig 7. Cell viability of AGS (Human gastric adenocarcinoma), MG-63, and Human Endothelial cell lines after being treated with different concentrations of MgFP5

3.3.2 ALP measurements

Measurement of ALP activity is important to assess the process of bone formation as well as mineralization. To verify the early differentiation, the osteoblast-like cell line SaOS-2 was treated with ionic dissolution products of MgFP bioactive glass, and the extracellular ALP secreted was assessed at 48 hours. The ALP measurement was determined by the colorimetric method at various concentrations (0.1 μg, 1 μg, 10 μg, 100 μg) compared to the control[13]. The results are graphically presented in Figure 8(**A**), represents a positive correlation between the concentration of MgFP bioactive glass and ALP activity.

3.3.3 Osteocalcin secretion

Osteogenic potential of the material can be directly determined by measuring the levels of osteocalcin. Increased levels of osteocalcin imply that the bioactive glass successfully stimulates osteoblast development and activity, which improves bone formation. Figure 8 (**B**) presents the osteocalcin levels measured by the ELISA method, both at intracellular and extracellular levels, in response to treatment with varying ionic dissolution concentrations of MgFP bioactive glass over 48 hours (100 μg/mL, 10 μg/mL, and 1 μg/mL). Mg^{2+} functions as a cofactor for enzymes that are involved in bone formation and mineralization processes by directly influencing the synthesis and activity of osteocalcin[14]. In the control group, the extracellular osteocalcin level is approximately 0.35 ng/mL, whereas the intracellular level is significantly lower, around 0.1 ng/mL. Extracellular osteocalcin levels increased distinctly to 0.5 ng/mL after the treatment with 1 μg/mL MgFP, while intracellular osteocalcin levels showed a slight increase to about 0.15 ng/mL. Increased osteoblastic activity and extracellular matrix mineralization are suggested by the particular increase in extracellular osteocalcin. The increase in intracellular osteocalcin may denote that the synthesis of osteocalcin is being upregulated in the cells. The increase in osteocalcin levels at 1 μg/mL which was reported is probably caused by the presence of Mg^{2+}. The extracellular osteocalcin level drops to around 0.35 ng/mL at 10 μg/mL MgFP, which is comparable to the control, while the intracellular level is mostly unchanged at about 0.1 ng/mL. This suggests that at this concentration, MgFP does not significantly enhance osteoblast activity compared to the control. Compared to the 1 μg/mL treatment, the reduced extracellular osteocalcin indicates a threshold effect where higher concentrations do not

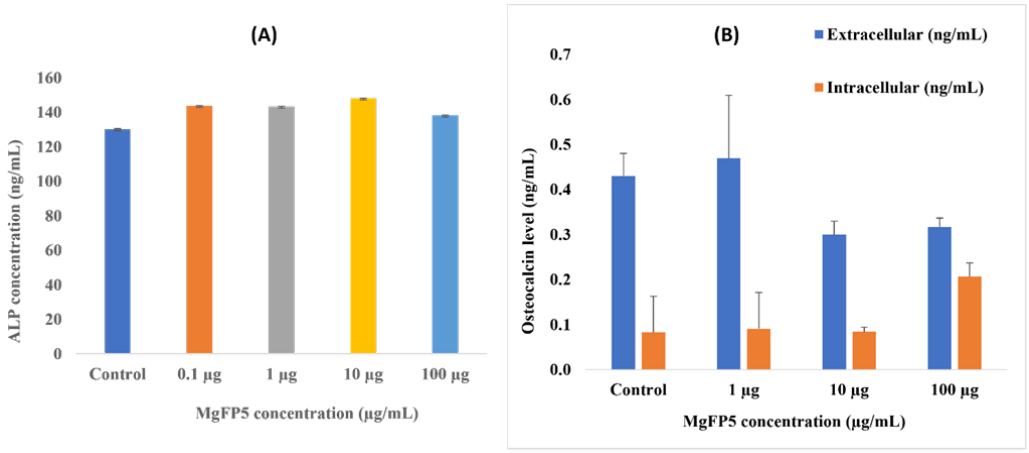

Fig 8. (A).Alkaline phosphatase activity of MgFP5 (B). Intracellular and extracellular osteocalcin levels of MgFP5

proportionally increase osteoblast activity which explains the ideal range of Mg^{2+} for osteoblast activity. Higher concentrations may cause cellular stress or inhibitory effects that lower osteocalcin synthesis. Osteocalcin levels extracellularly increase to around 0.4 ng/mL at the highest concentration of 100 μg/mL MgFP, whereas intracellular levels increase to about 0.15 ng/mL. The extracellular level at 100 μg/mL is lower than the 1 μg/mL treatment group, but it is still greater than the control and 10 μg/mL groups which indicates a possible biphasic response wherein moderate dosages are more effective which promotes the production and secretion of osteocalcin[13].

3.4 *In vivo* studies

The SEM image of the un-decalcified section of the femoral condyle of the rabbit at 100× magnification provides a thorough view of the morphological characteristics of the implanted nonporous MgFP bioactive glass and the subsequent bone conversion. The SEM image demonstrates the structural integrity and size of the implanted glass, as well as the gradual transformation occurring over 10 weeks. In Figure 9, the initial size of the nonporous MgFP bioactive glass rod is observed to decrease significantly because of the dissolution of the bioactive glass material. This dissolution facilitates the formation of an apatite layer by releasing ions such as Ca^{2+}, Na, and PO^{3-} along with Mg^{2+} into the physiological environment, which creates a well-defined interface between the glass and the bone. Mg^{2+} ions take part in nucleation and growth of hydroxyapatite ($Ca_{10}(PO_4)_6(OH)_2$), which is essential for bone bonding. The release of Mg^{2+} can enhance the crystallinity and mechanical properties of HAp which ensures a strong bond between the implant and the bone[15]. Over the 10-week *in vivo* study, the 2000 μm diameter rod was reduced to 1630 μm. This reduction is attributed to the combined effects of ion dissolution, bioactive glass resorption, and new bone formation at the interface zone. As seen in the SEM image at 1000× magnification, the distinct transformation layer around the bioactive glass implant represents the interface between the bone and the bioactive glass. This interface is the result of the integration of the implant with the bone. The EDS spectra reveal the elemental composition at the bone-bioactive glass interface. Peaks for P, Ca, Na, and O confirm the formation of new bone, indicative of mineralization processes. The rapid transformation and bonding ability of the glass to the bone is facilitated by these components. Mg^{2+} directly stimulates osteoblasts, which also increase the production of osteogenic markers such as collagen type I, osteocalcin, and alkaline phosphatase (ALP). To increase the proliferation and activity, it is necessary that these genes are expressed which results in the development of precursor cells into adult osteoblasts which in turn increase mineralization and formation of bone matrix[16].

In Figure 10, CLSM images exhibited the new bone development in a distinctive dark green fluorescence in the histological section, identified by calcein fluorescence. Within metabolically active cells, cellular esterases hydrolyze the non-fluorescent dye calcein AM to generate calcein, which fluoresces and stays in the cytoplasm. The intensity of this fluorescence is directly proportional to the activity of cellular metabolic activity, thereby providing a measure of cellular activity and bone formation. The rate of bioconversion was evidenced by the CLSM (Confocal Laser Scanning Microscopy) images illuminated by Ar laser, shown in brilliant fluorescence over the ring of the bone and interface which confirmed the depth of apatite formation extending up to 519 μm from the periphery of the implant which was measured at a fixed angle of 45° to the centre[17].

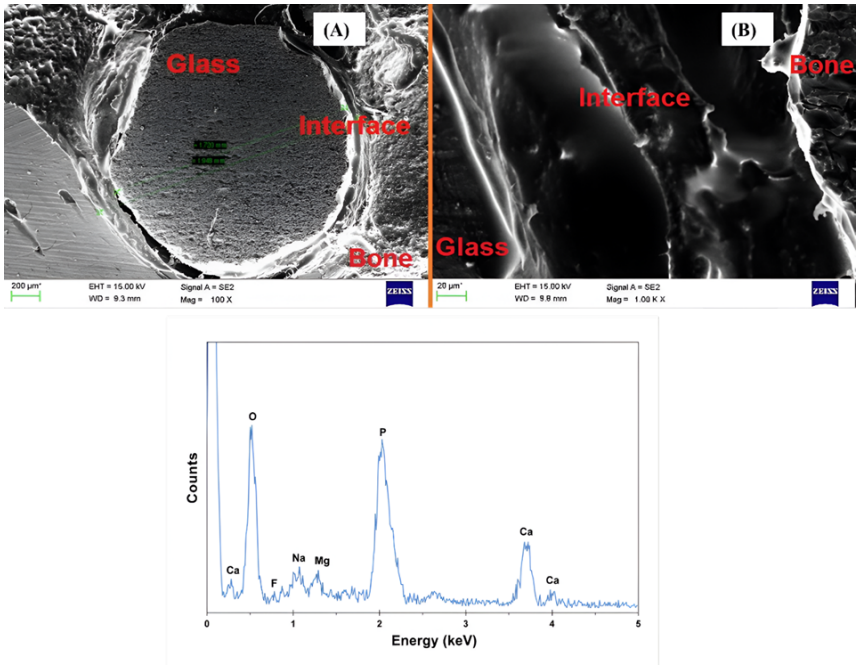

Fig 9. SEM_EDAX image of the undecalcified section of the implant (MgFP) in the cancellous bone of the rabbit after 10 weeks of implanting: (A) 100×; (B) 200× magnification

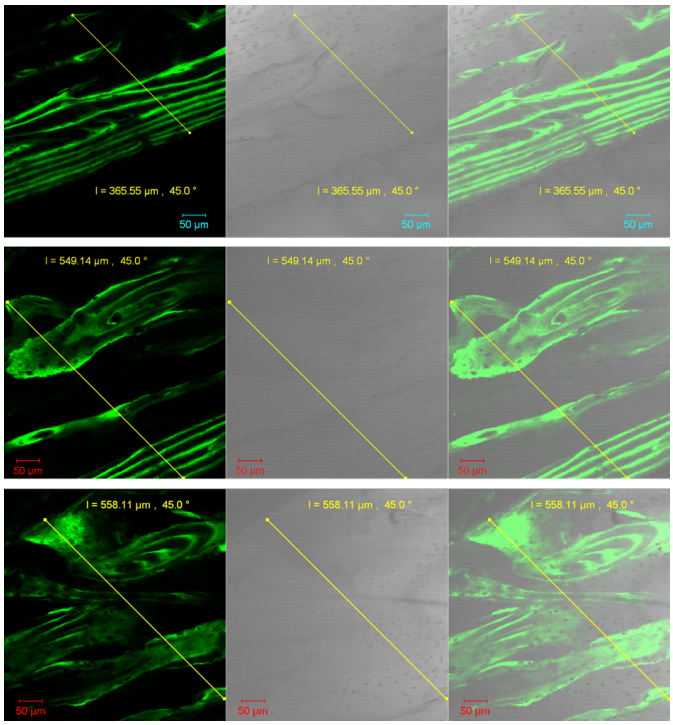

Fig 10. CLSM fluorescent images of the implant (MgFP5) at different depths

4 Discussion

It's a given that material science has been continuously used to produce synthetic biocompatible materials to accelerate bone repair and regeneration. Several formulations of bioactive glasses have been developed with the addition of therapeutic ions into their basic chemical composition. Many investigations have been reported to utilize the addition of therapeutic ions in silicate-based bioactive glasses but phosphate-based bioactive glasses with its melt-derived method of synthesis are explored less [18]. In this study, we have added magnesium (Mg and F^-) to phosphate-based bioactive glasses to prepare an osteogenic bone implant that can be integrated into living systems [9]. This study differs from our previous study using titanium (Ti) as a doped material wherein Ti-doped fluorophosphate bioactive glass focused on incremental fluoride doping to optimize structural integrity and biocompatibility. The other aspects of the discussion that differed from Mg-doped fluorophosphate bioactive glass were the material's inertness and osteoinductive properties that highlighted superior bonding and mechanical stability [19]. The present study is unique with the addition of different mol% of MgO which emphasized its dual role in biological stimulation and structural reinforcement with high reproducibility and controlled porosity. Mg is a non-toxic element that has the ability to get integrated into the living system. Mg is regarded as a nontoxic element for the human body at concentrations from 10 to 15 mM which promotes the proliferation and differentiation of osteoblasts and mesenchymal stem cells (MSCs) via the activation of MAPK/ERK signalling pathway and Notch1 signalling respectively. Pro-angiogenic capability is another add-on of Mg for its utilization in bone tissue engineering as it upregulates VEGF expression in human endothelial cells which in turn results in increased new blood vessel formation that leads to improved bone reconstruction *in vivo*. Despite this, it has been reported that exposure of Mg to artificial body fluids may lead to $MgCl_2$, MgO_2, and $Mg(OH)_2$ formation. But thankfully, these by-products are either excreted or incorporated into the natural metabolic process [20].

The addition of MgO to the fluorophosphate bioactive glasses positively influences the bioactive glass's dissolution rate as it gradually releases therapeutic ions and forms a HAp layer. In Figure 1 (**A**), XPS evaluation reveals that the calcium-to-phosphate (Ca/P) ratio and the presence of sodium-based compounds, such as $NaPO_3$ and Na_2O contribute to the apatite-forming ability and hydrophilic nature of the MgFP bioactive glasses [21]. All the substances listed in Table 2 are significant in the bone formation process. The role of calcium fluoride is particularly substantial which accelerated bone formation. In Figure 1(**B**), the variations in density values are likely due to modifications in the ceramic network. The increase in density at low MgO content suggests a denser packing or more efficient structural organization. The decrease in higher MgO content indicates a disruption in the phosphate network (breakage of the P–O–P bonds), possibly due to the formation of non-bridging oxygens (NBOs) which reduce the compactness of the glass network. The subsequent increase in density with higher MgO content could indicate that MgO starts to occupy interstitial positions or forms new phases that increase the overall density again but not to the initial peak value [22]. Figure 2 showed that Longitudinal, Bulk, Young's, and Shear moduli peak values indicated changes in the material's resistance to shear deformation with MgO content. From the observed results, MgFP5 was shown to maintain structural rigidity and was taken for thermal evaluation. In Figure 3, DSC and TG curves represented the sharp and distinctive endothermic peaks indicated a high degree of the material's purity. The TG curve (thermal stability) showed no weight loss up to around 1000°C which exhibited good thermal stability. The temperature window between the crystallization exotherm and the first endotherm is approximately 158.4°C (713.4°C - 555°C) which represents the range where the material is stable after crystallization but before melting [23].

In Figure 4, the replacement of MgO for Na_2O has been described to minimize the dissolution kinetics because of the greater Mg-O bond strength which explains the difference observed in the pH variation between MgFP5 and MgFP1. The lower pH observed in MgFP1 suggested a decreased ability to exchange Mg^{2+} ions with H^+ ions in the SBF. The calcium-phosphate (Ca-P) layer deposition and the formation of the HAp layer are significant which is impacted by the pH variations observed all through the immersion period [24]. For all the MgFP bioactive glass samples, the pH level did not cross a critical threshold due to the homogeneous nucleation of apatite formation. The pH plays a vital role in the healing mechanism, as an appropriate pH is required for the cross-linking of collagen chains and the precipitation of HAp which are essential for bone formation [25]. X-ray diffraction confirmed the formation of the new layer with associated compounds. After 21 days of *in vitro* degradation, the XRD patterns for Mg-doped fluorophosphate bioactive glasses with varying amounts of MgO are shown in Figure 5(**A**). In the obtained XRD shoulder peak at 32.19° and a weak one at 65.58° in the sample MgFP5 showed respectively the rich concentration of HAp and weak concentration of FAp which is suggestive of high crystallinity [26]. All the other samples had broader peaks with lower intensity expressing the crystallinity of the soaked sample. This characteristic peak at 25–35° range was considered as HAp which resembled natural bone apatite [27].

FTIR analysis in Figure 5(**B**) indicated that the carbonate substitution in the HAp is known to enhance bioactivity which is indicated by the peak at 870 cm^{-1} linked to C-O stretching. Symmetric P-O-P stretches, or the 720 cm^{-1} band, are a sign of pyrophosphate groups that support bone regeneration which adds to bioactivity. The detection of HAp confirms that all the bioactive glass samples possess bone-forming capabilities [28]. In Figure 6, SEM-EDS analysis showed that the deposited particle

sizes range from 20 to 100 nm. When the Ca/P ratio is below 1.3, the material exhibits high solubility, while a ratio above 1.3 results in decreased solubility. Initially, the calcium-to-phosphate ratio was 0.88, but after immersion, it increased to 1.46. This change indicates a significant difference in solubility and suggests the formation of calcium phosphate compounds, such as HAp, which are essential for bone bonding. The general charge in density and net polarity are influenced by the presence of elements like O, P, Ca, Na, Mg, and F. The interaction of these elements, particularly the higher electronegativity of O and F, contributes to the material's surface energy[29]. Mg plays a critical role in the substitution within the calcium-phosphate structure, often stabilize the amorphous phases and influence the crystallinity of the precipitated layer. The presence of Mg (1.74 atomic % before immersion) can influence the rate of HAp formation and improve the mechanical properties of the bioactive layer. This is another factor that the surface energy of the biomaterial influences protein and cell adhesion[30]. Therefore, substantial growth of HAp crystals is observable in the SEM micrograph of the MgFP5 sample. Figure 7 shows that the results of cell viability assay proposed that all the samples are cytocompatible at lower concentrations, which aligns with previous reports that mentioned that magnesium-doped bioactive glasses do not negatively affect cell compatibility[31]. However, additional investigations were conducted with higher concentrations (1, 10, and 100 μg/mL) of the samples. The quantitative results revealed that the cell viability decreased as the concentration of the sample increased. As the MgFP concentration increases from 1 μg/mL, to 100 μg/mL, the cell viability generally decreases, with the most significant reduction observed in the MG-63 and human endothelial cell line compared to the AGS cell line. The MG-63 and human endothelial cell lines exhibited better tolerance at 10 μg/mL of MgFP concentration. Moreover, the sample possessed significant cell viability (above 70%) even at higher concentrations (100 μg/mL). The independent t-test indicated significant differences in cell viability between the control and each cell line at various concentrations ($p<0.05$).

In Figure 8(**A**), it is shown that the SaOS-2 cell line produced ALP when incubated with the MgFP bioactive glass sample. 130 ng/mL was the baseline ALP activity for the control group. When compared to the control, the ALP level was higher in cells treated with the ionic dissolution products of the glass sample. At a concentration of 144 ng/mL, a slight increase in ALP activity was seen at 0.1 μg/mL which suggests that the bioactive glass induces osteogenic activity even at low concentrations. The ALP activity raised to 145 ng/mL at 1 μg concentration, which suggests a dose-dependent response. At 10 μg Concentration, the ALP activity peaked at around 148 ng/mL which indicates an optimal concentration for maximal osteogenic stimulation. The reason for this improvement is due to the ions released from the glass sample (PO_4^{3-}, Ca^{2+}, Mg^{2+}) could up-regulate the genes related to bone formation such as ALP and osteocalcin (OC). At 100 μg Concentration, the ALP activity slightly decreased to around 138 ng/mL, a potential saturation effect where higher concentrations do not significantly enhance or might inhibit the activity but the activity level was still above the control. The results are consistent with the previous findings, i.e., the positive effect of ions released (e.g., Mg^{2+}) from the bioactive glass on osteogenesis via the secretion of ALP[32]. The findings suggest that magnesium-doped fluorophosphate bioactive glass has significant potential for enhancing osteogenesis. In osteocalcin assay, Figure 8(**B**), shows that MgFP has a concentration-dependent effect on osteocalcin levels where the highest extracellular osteocalcin levels correspond to the 1 μg/mL concentration, which is the most effective that increases osteoblast activity. The intracellular measurements support the assumption of increased osteocalcin synthesis at 100 μg/mL concentration. Higher concentrations of MgFP (10 and 100 μg/mL) do not proportionally increase osteocalcin levels which suggests a possible saturation effect or negative feedback mechanism at play[33]. The results indicate the main significant differences between the control groups of extracellular and intracellular measurements ($p<0.05$).

In the *in vivo* studies, bone de-coring was prevented by using a trocar-tipped K wire, which also reduced peripheral osteocyte death caused by the heat generated during drilling. A cylindrical glass rod of 2 mm in diameter, was used to eliminate the gap between the drilled hole and the implant. With the space between the implant and the hole being virtually non-existent, the bioconversion could be directly linked to the effects of the ionic dissolution products of the glass on the host cells and the penetration of live cells over the implanted material[34]. Mg^{2+} promotes angiogenesis that leads to increased vascularization which provides necessary nutrients and oxygen, supporting bone growth and healing. Osteoclasts responsible for bone resorption, can also be inhibited by Mg^{2+} ions. This inhibition favors net bone acquisition by preserving the equilibrium between bone production and resorption. The SEM image in Figure 9 exhibits the structural integrity and size of the implanted glass and the gradual transformation which occured over 10 weeks. The fluorescent green areas in the histological sections indicate zones of partially mineralized bone, emphasizing the presence and extent of new bone formation at the interface. No voids were observed between the glass and bone, with uniform contact maintained at various points along the interface. The fluorescence intensity and distribution (Figure 10) demonstrate the active role of the MgFP bioactive glass which promotes bone regeneration. The presence of Mg^{2+} ions along with Ca^{2+}, PO_4^{3-}, Na^{2+}, F^{-}, and O in the MgFP bioactive glass enhances osteogenic differentiation and proliferation[35]. The area of bioconversion was calculated using the following formula:

$$\text{Area of bioconversion} = \frac{3.143(R.R) - 3.143(r.r)}{3.143(R.R)} \text{ X } 100$$

where R = radius of implant; X = radius of conversion; r = R-X = radius of residual implant

The bioconversion area calculated using this formula indicates significant transformation, with approximately 67% of the nonporous rod undergoing bioconversion within 10 weeks. Hence, the presence of Mg^{2+} ions not only accelerate the formation of new bone but also ensures that the new bone formed is of high quality and capable of withstanding physiological stresses [36]. Therefore, it can be concluded that implanted MgFP bioactive glass rod favours bone formation within 10 weeks at molecular levels post-surgery [37].

5 Conclusion

The present study has demonstrated the applicability of novel combination of processing method i.e. melt-quenching based on the maximum advantages which include better scalability, reproducibility, purity of the glasses, superior mechanical strength, and cost-effective over silicate-based systems as reported in the literature as well as doping with therapeutic ions such as Mg, and F^- the melt-derived phosphate-based bioactive glass (P_2O_5-CaO-CaF_2-Na_2O-MgO) as a bone graft for tissue engineering. The longitudinal, shear, Young's, and bulk moduli of the bioactive glasses showed a trend that correspond to the variations in density. Specifically, at 5 mol% MgO, the density, longitudinal, shear, Young's, and bulk moduli were measured as 2645 kg/m^3, 67.2GPa, 18.87GPa, 49.1GPa, and 47GPa respectively. This structural integrity of the material was confirmed by the correlation between elastic properties and density measurements. XPS revealed the presence of calcium fluorophosphate groups which indicated successful fluoride incorporation essential for bioactivity. The bioactivity of the MgFP glasses was confirmed by their ability to form apatite on the surface when immersed in simulated body fluid (SBF). A high level of HAp formation at 31.92° in XRD analysis denoted successful conversion from amorphous to crystalline phase. EDS analysis confirmed the presence of essential elements which include Mg and F, with a Ca/P ratio of 1.46 aligning with natural HAp which is essential for bone bonding. HAp and FAp was crucial for the implant's anchorage to the host bone, observed significantly in all samples (MgFP1–MgFP5). *In vitro* studies demonstrated the non-toxic nature of MgFP bioactive glass at various concentrations which maintain high cell viability in AGS, MG-63, and human endothelial cell lines which exhibited 86%, 88%, and 80% respectively at 0.1μg, 10μg, and 0.1μg. Alkaline phosphatase (ALP) and osteocalcin assays showed increased levels than the control which indicated enhanced osteogenic properties. Among the tested samples, MgFP5 which contains 5 mol% MgO *in vivo* evaluation. *In vivo* studies on rabbit femoral condyles revealed significant bone formation, with the MgFP5 sample showed within 10 weeks, as observed in SEM and CLSM analyses highlight the effectiveness of the melt-derived Mg-doped fluorophosphate bioactive glasses in critical load-bearing bone defect repairs. No voids were observed during *in vivo* studies which confirmed that the resorption and new bone formation occurred at the same rate, a critical attribute of an ideal bone substitute. These findings confirm the material's effectiveness in promoting bone regeneration and its potential use in bone tissue engineering. Further studies are recommended to conduct extensive clinical trials in human subjects to validate the performance of the material patient-specific targeted therapy to ensure its safety and efficacy in various clinical scenarios.

Acknowledgements

The authors thank Dr. G. Kumaresan, Associate Professor and Head of the Department of Genetics at the Centre for Excellence in Genomic Sciences, School of Biological Sciences, Madurai Kamaraj University, Madurai, India, for his assistance with the cell viability evaluation. They also acknowledge the financial support from M/S Pandian Advanced Medical Centre Private Limited, Madurai, India, provided for this work.

References

1) Awad HA, Keefe RJ, Mao JJ. Bone tissue engineering. In: and others, editor. Principles of Tissue Engineering. Academic Press. 2020;p. 1511–1519. Available from: https://doi.org/10.1016/B978-0-12-818422-6.00083-6.
2) Li Y, Chen L, Chen X, Hill R, Zou S, Wang M, et al. High phosphate content in bioactive glasses promotes osteogenesis in vitro and in vivo. *Dental Materials*. 2021;37(2):272–283. Available from: https://doi.org/10.1016/j.dental.2020.11.017.
3) Sankaralingam PP, Sakthivel P, Thangavel VC. Bioceramics for Regenerative Medicine. In: Hoque ME, Goh KL, Sagadevan S, et al., editors. Advanced Bioceramics- Properties, Processing, and Applications. Boca Raton. CRC Press. 2023;p. 1–21. Available from: https://www.taylorfrancis.com/chapters/edit/10.1201/9781003258353-14/bioceramics-regenerative-medicine-pugalanthi-pandian-sankaralingam-poornimadevi-sakthivel-vijayakumar-chinnaswamy-thangavel?context=ubx&refId=b47ebf6f-55f6-48f3-92e9-b5b7575bad56.
4) Shoaib M, Bahadur A, Iqbal S, Al-Anazy MM, Laref A, Tahir MA, et al. Magnesium doped mesoporous bioactive glass nanoparticles: A promising material for apatite formation and mitomycin c delivery to the MG-63 cancer cells. *Journal of Alloys and Compounds*. 2021;866. Available from: https://doi.org/10.1016/j.jallcom.2021.159013.
5) Sankaralingam P, Sakthivel P, Thangavel VC. Novel Composites for Bone Tissue Engineering. In: Haidar ZS, et al., editors. Biomimetics - Bridging the Gap. 2022. Available from: https://www.intechopen.com/chapters/83092.

6) Kokubo T, Takadama H. Simulated Body Fluid (SBF) as a Standard Tool to Test the Bioactivity of Implants. In: Bäuerlein PDE, et al., editors. Handbook of biomineralization: biological aspects and structure formation. 2007;p. 97–109. Available from: https://doi.org/10.1002/9783527619443.ch51.
7) Sankaralingam P, Sakthivel P, Subbiah PA, Periyasamy A, Rahumathullah JB, Thangavel VC. Fluorophosphate bio-glass for bone tissue engineering: in vitro and in vivo study. Thomas Telford Ltd.. 2021. Available from: https://dx.doi.org/10.1680/jbibn.21.00025. doi:10.1680/jbibn.21.00025.
8) Möncke D, Eckert H. Review on the structural analysis of fluoride-phosphate and fluoro-phosphate glasses. *Journal of Non-Crystalline Solids: X*. 2019;3. Available from: https://dx.doi.org/10.1016/j.nocx.2019.100026.
9) Mocanu A, Cadar O, Frangopol PT, Petean I, Tomoaia G, Paltinean GA, et al. Ion release from hydroxyapatite and substituted hydroxyapatites in different immersion liquids: In vitro experiments and theoretical modelling study. *Royal Society open science*. 2021;8. Available from: https://doi.org/10.1098/rsos.201785.
10) Akhrouf A, Krimi S, Abdouni IE. Impact of CaO addition on physico-chemical properties, crystallization, chemical durability and in vitro behavior of Na2O-ZnO-TiO2-P2O5 glasses. *Inorganic Chemistry Communications*. 2023;158(2). Available from: https://doi.org/10.1016/j.inoche.2023.111602.
11) Arepalli SK, Tripathi H, Manna PP, Pankaj P, Krishnamurthy S, Patne SC, et al. Preparation and in vitro investigation on bioactivity of magnesia-contained bioactive glasses. *Journal of the Australian Ceramic Society*. 2019;55:145–155. Available from: https://link.springer.com/article/10.1007/s41779-018-0220-5.
12) Uppal G, Thakur A, Chauhan A, Bala S. Magnesium based implants for functional bone tissue regeneration-A review. *Journal of Magnesium and Alloys*. 2022;10(2):356–386. Available from: https://doi.org/10.1016/j.jma.2021.08.017.
13) Moghanian A, Sedghi A, Ghorbanoghli A, Salari E. The effect of magnesium content on in vitro bioactivity, biological behavior and antibacterial activity of sol-gel derived 58S bioactive glass. *Ceramics international*. 2018;44(8):9422–9432. Available from: https://doi.org/10.1016/j.ceramint.2018.02.159.
14) Kargozar S, Lotfibakhshaeish N, Ebrahimi-Barough S, Nazari B, Hill RG. Stimulation of osteogenic differentiation of induced pluripotent stem cells (iPSCs) using bioactive glasses: an in vitro study. *Frontiers in Bioengineering and Biotechnology*. 2019;7. Available from: https://pubmed.ncbi.nlm.nih.gov/31850324/.
15) Kargozar S, Milan PB, Amoupour M, Kermani F, Gorgani S, Nazarnezhad S, et al. Osteogenic potential of magnesium (Mg)-doped multicomponent bioactive glass: in vitro and in vivo animal studies. *Materials*. 2022;15(1). Available from: https://doi.org/10.3390/ma15010318.
16) Hohenbild F, Ospina MA, Schmitz SI, Moghaddam A, Boccaccini AR, Westhauser F. An in vitro evaluation of the biological and osteogenic properties of magnesium-doped bioactive glasses for application in bone tissue engineering. *International Journal of Molecular Sciences*. 2021;22(23). Available from: https://pubmed.ncbi.nlm.nih.gov/34884519/.
17) Qi X, Wang H, Zhang Y, Pang L, Xiao W, Jia W, et al. Mesoporous bioactive glass-coated 3D printed borosilicate bioactive glass scaffolds for improving repair of bone defects. *International Journal of Biological Sciences*. 2018;14(4):471–484. Available from: https://pmc.ncbi.nlm.nih.gov/articles/PMC5930479/.
18) Baino F, Hamzehlou S, Kargozar S. Bioactive glasses: where are we and where are we going. *Journal of functional biomaterials*. 2018;9(1). Available from: https://pubmed.ncbi.nlm.nih.gov/29562680/.
19) Sankaralingam PP, Sakthivel P, Subbiah PA, Rahumathulla J, Thangavel VC. Preparation and physical-biological characterization on titanium doped fluorophosphate nanobioglass: Bone implants. *International Journal of Ceramic Engineering & Science*. 2021;3(1):37–48. Available from: https://doi.org/10.1002/ces2.10078.
20) ElBatal HA, Khalil EMA, Hamdy YM. In vitro behavior of bioactive phosphate glass–ceramics from the system P2O5–Na2O–CaO containing titania. *Ceramics International*. 2009;35(3):1195–1204. Available from: https://dx.doi.org/10.1016/j.ceramint.2008.06.004.
21) Anand A, Kaňková H, Hájovská Z, Galusek D, Boccaccini AR, Galusková D. Bio-response of copper-magnesium co-substituted mesoporous bioactive glass for bone tissue regeneration. *Journal of Materials Chemistry B*. 2024;12(7):1875–1891. Available from: https://pubs.rsc.org/en/content/articlelanding/2024/tb/d3tb01568h.
22) Ebrahimi M, Manafi S, Sharifianjazi F. The effect of Ag2O and MgO dopants on the bioactivity, biocompatibility, and antibacterial properties of 58S bioactive glass synthesized by the sol-gel method. *Journal of Non-Crystalline Solids*. 2023;606. Available from: https://dx.doi.org/10.1016/j.jnoncrysol.2023.122189.
23) Kaur G, Kumar V, Baino F, Mauro JC, Pickrell G, Evans I, et al. Mechanical properties of bioactive glasses, ceramics, glass-ceramics and composites: State-of-the-art review and future challenges. *Materials Science and Engineering: C*. 2019;104. Available from: https://dx.doi.org/10.1016/j.msec.2019.109895.
24) Demir-Oğuz Ö, Boccaccini AR, Loca D. Injectable bone cements: What benefits the combination of calcium phosphates and bioactive glasses could bring? *Bioactive Materials*. 2023;19:217–236. Available from: https://dx.doi.org/10.1016/j.bioactmat.2022.04.007.
25) Rajkumar G, Dhivya V, Mahalaxmi S, Rajkumar K, Sathishkumar GK, Karpagam R. Influence of fluoride for enhancing bioactivity onto phosphate based glasses. *Journal of Non-Crystalline Solids*. 2018;493:108–118. Available from: https://doi.org/10.1016/j.jnoncrysol.2018.04.046.
26) Erasmus EP, Sule R, Johnson OT, Massera J, Sigalas I. In vitro Evaluation of Porous borosilicate, borophosphate and phosphate Bioactive Glasses Scaffolds fabricated using Foaming Agent for Bone Regeneration. *Scientific Reports*. 2018;8. Available from: https://dx.doi.org/10.1038/s41598-018-22032-2.
27) Hajiali F, Tajbakhsh S, Shojaei A. Fabrication and Properties of Polycaprolactone Composites Containing Calcium Phosphate-Based Ceramics and Bioactive Glasses in Bone Tissue Engineering: A Review. *Polymer Reviews*. 2018;58(1):164–207. Available from: https://dx.doi.org/10.1080/15583724.2017.1332640.
28) Montazerian M, Shearer A, Mauro JC. Perspectives on the impact of crystallization in bioactive glasses and glass-ceramics. *International Journal of Ceramic Engineering & Science*. 2024;6(1). Available from: https://dx.doi.org/10.1002/ces2.10194.
29) Nommeots-Nomm A, Houaoui A, Packiyanathar AP, Chen X, Hokka M, Hill R, et al. Phosphate/oxyfluorophosphate glass crystallization and its impact on dissolution and cytotoxicity. *Materials Science and Engineering: C*. 2020;117. Available from: https://dx.doi.org/10.1016/j.msec.2020.111269.
30) Seyedmajidi S, Seyedmajidi M, Zabihi E, Hajian-Tilaki K. A comparative study on cytotoxicity and genotoxicity of the hydroxyapatite-bioactive glass and fluorapatite-bioactive glass nanocomposite foams as tissue scaffold for bone repair. *Journal of Biomedical Materials Research Part A*. 2018;106(10):2605–2612. Available from: https://dx.doi.org/10.1002/jbm.a.36452.
31) Dai Q, Wang Z, Liu C, Chen X, Cao X. High performance injectable Mg doped bioactive glass bone cement for the regulation of osteogenic immune microenvironment. *Biomaterials Advances*. 2024;160. Available from: https://doi.org/10.1016/j.bioadv.2024.213864.
32) Rajendran AK, Anthraper MS, Hwang NS, Rangasamy J. Osteogenesis and angiogenesis promoting bioactive ceramics. *Materials Science and Engineering: R: Reports*. 2024;159. Available from: https://doi.org/10.1016/j.mser.2024.100801.
33) Lin Q, Zhang X, Wang W, Li S, Li J, Hao L. The structural evolution of Bioglass after implantation in the femoral defects. *Journal of Non-Crystalline Solids*. 2021;552. Available from: https://doi.org/10.1016/j.jnoncrysol.2020.120439.
34) Zhou H, Liang B, Jiang H, Deng Z, Yu K. Magnesium-based biomaterials as emerging agents for bone repair and regeneration: From mechanism to application. *Journal of Magnesium and Alloys*. 2021;9(3):779–804. Available from: https://www.sciencedirect.com/science/article/pii/S2213956721000578.

35) Xu L, Willumeit-Römer R, Luthringer-Feyerabend BJC. Effect of magnesium-degradation products and hypoxia on the angiogenesis of human umbilical vein endothelial cells. *Acta Biomaterialia*. 2019;98:269–283. Available from: https://doi.org/10.1016/j.actbio.2019.02.018.
36) Rajkumar G, Pugalanthipandian S. Bioconversion of magnesium added fluorophosphate glass and method of making thereof. WIPO. 2013. Indian Patent WO2015092815. Available from: https://patentscope.wipo.int/search/en/detail.jsf?docId=WO15/092815.
37) Kaou MH, Furkó M, Balázsi K, Balázsi C. Advanced bioactive glasses: the newest achievements and breakthroughs in the area. *Nanomaterials*. 2023;13(16). Available from: https://doi.org/10.3390/nano13162287.